New understanding of TeO2–ZnO–Na2O ternary glass system

Jonathan de Clermont-Gallerande, Shunsuke Saito, Maggy Colas, Philippe Thomas, Tomokatsu Hayakawa

New understanding of TeO_2-ZnO-Na_2O ternary glass system.

Jonathan de Clermont-Gallerande[1]; Shunsuke Saito[1]; Maggy Colas[2]; Philippe Thomas[2]; Tomokatsu Hayakawa[1,3,*]

[1]Field of Advanced Ceramics, Department of Life Science and Applied Chemistry, Nagoya Institute of Technology, Gokiso, Showa, Nagoya 466-8555, Japan
[2]Institut de recherche sur les céramiques (IRCER), UMR 7315 CNRS / Université de Limoges, Centre Européen de la Céramique, 12, rue Atlantis, 87068 Limoges, France
[3]Frontier Research Institute of Materials Science (FRIMS), Nagoya Institute of Technology, Gokiso, Showa, Nagoya 466-8555, Japan
*corresponding author: hayatomo@nitech.ac.jp

Abstract

Thermal, mechanical structural and optical properties of the 80TeO_2-xZnO-(20-x)Na_2O (TZN) system were investigated. The structural study of the glasses showed that in the TZN system, the zinc had a coordination and hence a behavior change in the tellurite matrix as a function of the concentration. Those results were correlated to the elastic properties of the glasses, like the Young modulus, the shear modulus and the Poisson ratio, thermal properties with the index of thermal stability and the crystallization behavior and the optical properties of refractive index which presented nonlinear evolutions as a function of the ZnO concentration. An in-depth study of the Boson peak is proposed with a study on the correlation length, here named as the blob size, performed from its evolution and the evolution of the mechanical properties.

Introduction

Tellurite glasses have interested not only material researchers but also device developers in the field of photonics for many years. Indeed, they are good candidates for photonic applications thanks to their high linear refractive index, high dielectric constant, wide infrared transmittance, and their high third order non-linear optical susceptibilities(1–4).

Ab-initio studies showed that the pure TeO_2 glass has the highest non-linear optical properties among tellurite glasses (5) (fifty times more than fused silica glasses (4,6)), but extreme quenching conditions are needed to obtain the glass (7). Consequently, modifier oxides are required to be added. A variety of multicomponent tellurite glass systems have been studied in their abilities to form glasses (glassy domains) and their structural, linear and non-linear optical properties for many years (8–16). Among them, adding Na_2O is well known to increase the glass forming ability resulting in homogeneous glasses with only slight modifications of TeO_2 glass structure (8,15,16).

Adding ZnO in tellurite glasses significantly increases the glass forming domain (up to 40%mol ZnO) (17). Binary TeO_2-ZnO glasses are useful media for ultra-low loss optical fibers (1 dB/km) in the wavelength range of 3.4-4 µm (18). Different studies have been done on TeO_2-ZnO glasses based on Raman spectroscopic data (19–24), and X-ray absorption fine structure (XAFS) (25). The studies showed that adding ZnO to the original TeO_2 glass matrix results in *(i)* a structural transformation of trigonal bipyramids TeO_4 into trigonal pyramid TeO_3 units and so a linear decrease of the optical properties; *(ii)* a band gap decrease as the glasses turn more transparent upon adding ZnO (26); *(iii)* a change in the Zn-O coordination (6-coordinated for low concentration of ZnO and 4-coordinated for high concentrations of

ZnO) and structural behaviors (between the tellurite chains when 6-coordinated and substituting the TeO_2 inside the chains when 4-coordinated) (24).

The goal of the present study is to highlight new discoveries in the $80TeO_2$-xZnO-(20-x)Na_2O (x = 0, 5, 10, 15, 20%mol) (TZN) ternary system in accordance to thermal, mechanical, structural and optical properties. In this paper, the short and medium-range structure of TZN glasses is reported using Raman spectroscopy, mechanical properties by ultrasound echography (27), thermal properties by differential thermal analysis (DTA) experiment and optical properties by UV(ultraviolet)-visible-infrared spectroscopy and refractometer. The TZN glasses were also doped with 0.5%wt Nd^{3+} ions to study photoluminescent properties of the glasses, which will be reported elsewhere. As the doping was small, the structural data given in this paper for the TZN glasses with different ZnO concentration are not affected by the Nd^{3+} ions (28). Low-frequency Raman spectroscopy is applied to gain structural information of medium range of orders for the TZN glasses with constant TeO_2 content 80%mol and varying ZnO content from 0 to 20%mol, which shed light on how the network evolution of tellurite glasses is influenced by ZnO (covalent) and Na_2O (ionic) entities.

1. Experimental

1.1. Sample preparation

The relevant amount (2g) of the different initial powders (α-TeO_2 obtained by the decomposition of telluric acid (Aldrich): anhydrous Na_2CO_3 (Asahi Glass Co.): ZnO (Kishida Chem. Co.)) within the ternary system $80TeO_2$-xZnO-(20-x)Na_2O, with x= 0; 5; 10; 15 and 20%mol (respectively named TZ0N20, TZ05N15, TZ10N10, TZ15N05 and TZ20N0) were ground in a mortar for 30 minutes and then melted in a platinum crucible at 850°C for one hour before being quenched on a 8mm diameter brass mold preheated at ~100°C. The obtained glasses were optically polished with a 2mm thickness after they were annealed at 30°C below the glass transition temperature (Tg) for 12 hours in order to release stresses resulting from the rapid quenching of melt. The final concentrations of the samples have been controlled by energy dispersive X-ray spectroscopic (EDS; JEOL, JSL-6010LA) experiments which evidence a deviation less than 2% from the theoretical composition. The obtained glasses were ground only for thermal analysis and Raman spectroscopy measurements.

Thermal properties were measured by DTA experiments with a RIGAKU TGD9600 in a Pt pan at a 10°C/min rate in a 100~700°C temperature range. Density measurements were done by the Archimedes method. Raman spectra were recorded in the 1.7-950cm^{-1} spectral range, using a JASCO NRS-2000 spectrometer at 532 nm excitation at ~30 mW. The mechanical properties have been obtained by ultrasound echography (Olympus, 5072PR). UV-Vis-IR measurements were recorded on JASCO V-570 spectrometer. The refractive index was taken by a refractometer (Five-lab, Mary-102).

2. Results and discussion

2.1. Thermal properties and density measurements

The DTA curves are presented in Figure 1 and the relevant information (Glass transition temperature Tg, on-set crystallization temperature Tx, first crystallization peak Tc and the

index of thermal stability ΔT (=Tx-Tg)) are reported on Table 1. The density data were also added to the Table 1 for indication.

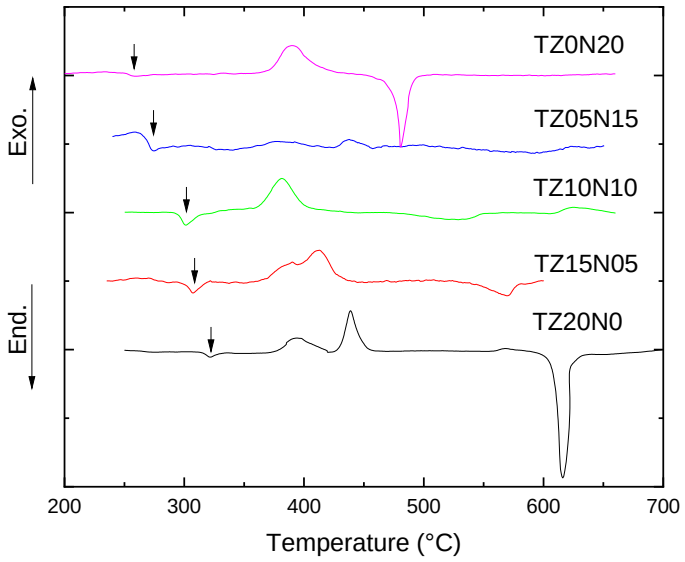

Figure 1 : DTA evolution for every TZN samples. The arrow shows the respective glass transition temperature.

Sample	Tg (°C)	Tx (°C)	Tc (°C)	ΔT (°C)	Density, *d* (g/cm^3)	Molar Volume / cm^3 mol^{-1}	Refractive index, *n*
TZ0N20	250	363	390	113	4.89 ± 0.01	2867 ± 4	1.976 ± 0.037
TZ5N15	264	345	374	81	5.03 ± 0.01	2801 ± 8	1.952 ± 0.007
TZ10N10	299	359	381	67	5.35 ± 0.01	2664 ± 3	2.030 ± 0.006
TZ15N5	298	361	390	63	5.35 ± 0.01	2671 ± 4	2.013 ± 0.002
TZ20N0	312	371	394	59	5.53 ± 0.05	2602 ± 23	2.033 ± 0.002

Table 1 : Tg, Tx, Tc and ΔT (± 1 °C) as well as density, molar volume and refractive index of TZN glasses

Figure 1 shows that with an increase of the zinc oxide concentration from 0 to 5%mol, there is a sharp decrease of the crystallization peak intensity. For further increase of the zinc oxide concentration, two different crystallization peaks appear with temperature increases. Those peaks are more defined with an increase of zinc oxide concentration. With an increase of zinc oxide content, it can also be seen in Table 1 that there is an increase of the glass transition temperature and a sharp decrease of the thermal stability for concentrations higher than 5%mol of zinc oxide.

The density increases linearly with an increase of the zinc oxide concentration except 10%mol of zinc oxide. This evolution is almost in line with the Tg evolution as a function of the concentration. The molar volume is given from the experimental value of density and the formal composition, which is tabulated in Table 1.

2.2. Raman spectroscopy

All Raman spectra were normalized (total area normalization) and baseline corrected (linear correction).

The normalized spectra were then decomposed using the Focus program (29) based on previous studies (10,26,30), with 10 oscillators: 9 Gaussian functions and 1 log-normal function. Due to the width and overlapping of the bands of the normalized Raman spectra (Figure 2) all Gaussian functions had full width at half maximum (FWHM) and frequency fixed, and only the intensity was left free. As the log-normal function is well defined, all fitting parameters were left totally free (frequency, FWHM and intensity).

The TZN glass Raman spectra's frequencies range can be divided in two different parts: the low wavenumber region with the Boson peak (BP) and the high wavenumber region (300-800 cm^{-1}) with the deformation of bridges (asymmetric and symmetric Te-O-Te) and the elongation vibrations of Te-O bonds for TeO_3 and TeO_4 polyhedra (Figure 2).

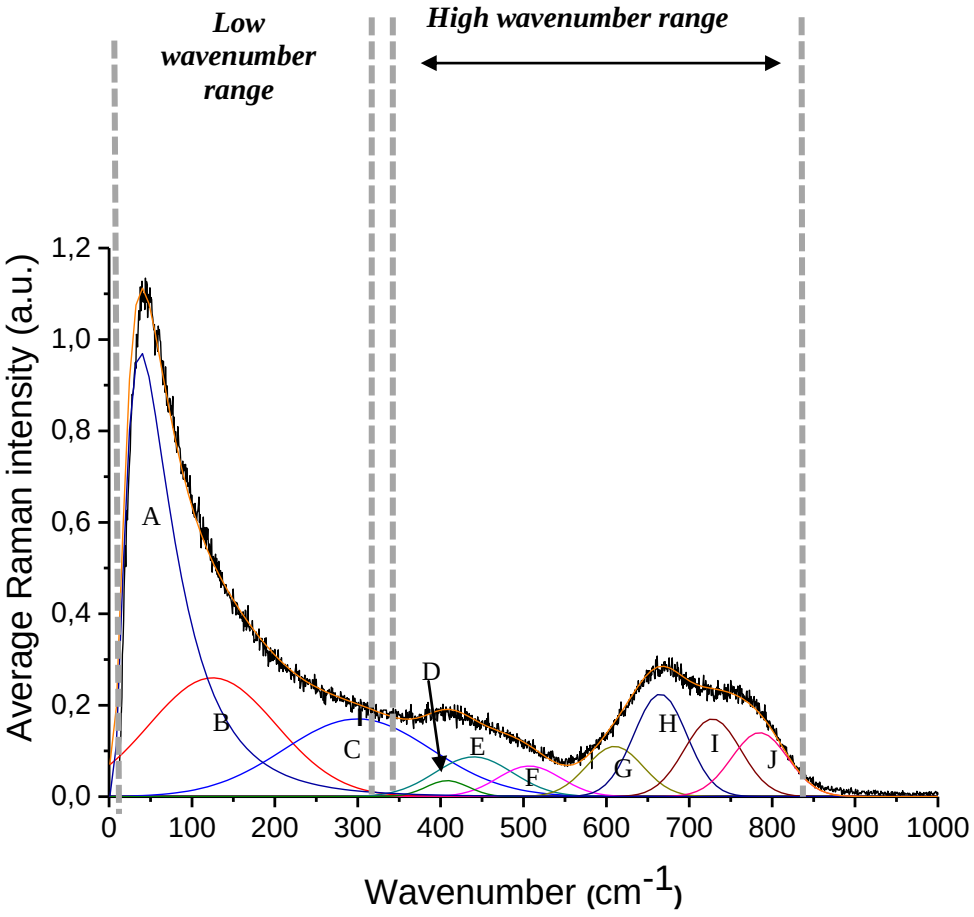

Figure 2 : Raman bands attribution of a typical TZN sample (Example of the TZ15N05 sample)

Frequency (cm^{-1})	Attribution
A (~60)	Boson peak
E (~440)	Symmetric elongation of Te-O-Te bridges
F (~500)	Asymmetric elongation of Te-O-Te bridges
G (~610)	Non-symmetric elongation of Te-O bonds in TeO_4 polyhedra
H (~660)	Symmetric elongation of Te-O bonds in TeO_4 and TeO_3 polyhedra
I (~720)	Non-bridging elongation of Te-O (NBO) bonds in TeO_3 polyhedra
J (~780)	Non-bridging elongation of Te-O (NBO) bonds in TeO_4 polyhedra

Table 2 : Frequencies and mode attribution of the used oscillators for the decomposition of the TZN Raman spectra. NBO: Non-bridging oxygen

2.2.1. Study of the high wavenumber region

Figure 3 shows the structural evolution of the high wavenumber bands as a function of the concentration. When looking at the bands associated with the Te-O-Te bonds elongation (Fig. 3a) there is an overall increase of the intensity of the band associated to the symmetric elongation of Te-O-Te bridges (band E) and a decrease of the intensity of the band associated to the asymmetric elongation Te-O-Te bridges (band F). When looking at the bands associated with the TeO_3 and TeO_4 elongation (Fig. 3b), it can be seen that for concentrations lower than 10%mol ZnO there is a decrease of the intensity non-bridging elongation of Te-O (NBO) bonds in TeO_3 and TeO_4 polyhedra (band I and J) and for higher concentration an increase of the intensity of the same bands. There is also a linear decrease of the non-symmetric elongation of Te-O bonds in TeO_4 polyhedra (band G) and between 0 and 5%mol ZnO a slight increase of the intensity of the band associated to the symmetric elongation of Te-O bonds in TeO_4 and TeO_3 polyhedra (band H) and a decrease of its intensity for higher concentrations.

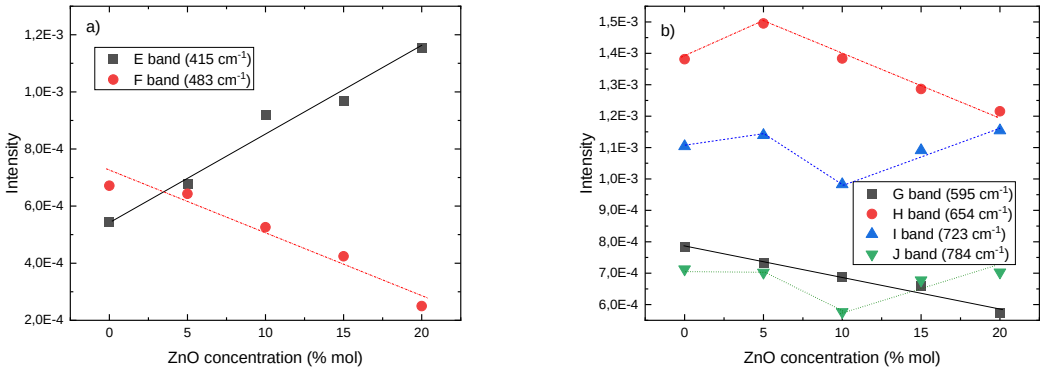

Figure 3 : Intensity evolution of a) E and F bands and b) G, H, I and J bands as a function of the ZnO concentration

The complete analysis of the evolution of the high wavenumber region become more relevant by looking at the TeO_3/TeO_4 ratio, which should give an idea on the depolymerization of the tellurite network. This ratio is calculated from the following equation:

$(I_I+I_H)/(I_J+I_H+I_G)$, I being the intensity of the corresponding bands. Its evolution with an increase amount of ZnO is shown in Figure 4.

The TeO_3/TeO_4 ratio is overall increasing with an increase of the ZnO content, but between 5 and 15%mol ZnO the ratio is almost constant. This means that between these concentrations, there is a change in structural behavior in this range of concentrations.

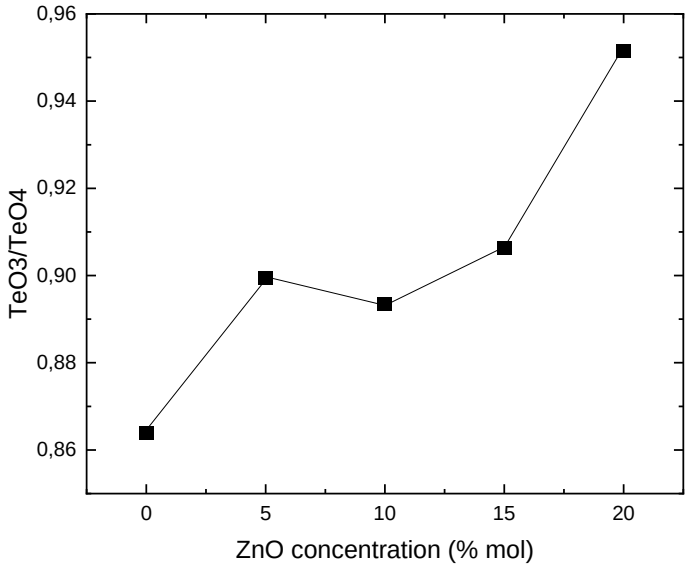

Figure 4 : Evolution of the TeO_3/TeO_4 ratio as a function of the ZnO concentration

By looking at the evolution of the different bands inside the high wavenumber region and comparing it to the literatures, it is possible to understand the present evolution of intensity.

- For concentrations lower than 5%mol ZnO there is an increase of TeO_3 because of the introduction of ZnO (band F more intense than band E, slight increase of band H, strong increase of the TeO_3/TeO_4 ratio). This means that the ZnO is behaving like a modifier. It can be explained by the low content of ZnO.
- For concentration between 5 and 10%mol ZnO, a slight decrease of the TeO_3/TeO_4 ratio and a decrease of the I and J band intensity is noted. By comparing these results to the literatures (19–21,23–26), it is possible to hypothesize that for concentrations lower than 10%mol ZnO the zinc oxide will be octahedra formed and between the chains, linking to the network, decreasing the number of NBO, and slightly increasing the network polymerization.
- For concentration higher than 10%mol ZnO, there is an increase of the TeO_3/TeO_4 ratio and an increase of the intensity of the I and J bands. This shows a change in the structural behavior, with a change of the zinc coordination, going toward tetrahedra formed, and substituting the tellurium oxide inside the chains (24). With higher the concentration of ZnO, there will be more tetrahedra formed ZnO, increasing the TeO_3/TeO_4 ratio and the number of NBO.

For better understanding of the structural changes, it is interesting to look at the low wavenumber region and more specifically at the Boson peak (BP).

2.2.2. Study of the low wavenumber region

Non-crystalline materials (glasses and amorphous solids) have notable differences compared to crystalline solids in vibratory dynamics around 1THz (33,3 cm^{-1}) (31). Those low energy excitation are used in different cases and among them it is used for explaining the presence of dispersed intensities, which are not present inside parent crystals on Raman spectra and incoherent neutron diffusion (INS) (31–33).

This point has been researched for a number of years theoretically or experimentally (34–48). Unfortunately, after more than four decades of research, the origin of this peak, named 'Boson peak', because the vibrational population of the energetic levels of this peak was dependent on the temperature following the Bose-Einstein statistical prediction, is still not satisfactorily explained.

Because it is difficult to establish one unique theory valid for all glasses, empiric correlations were established from their properties. Indeed, one spectral characteristic of the Boson peak (intensity, position …) is correlated to a specific property of the glass. But even these empiric correlations are dispersed. The Boson peak is associated with different models: *(i)* The dispersion of acoustic phonons in a disordered medium by polarizability (49) ; *(ii)* The fluctuation of the intrinsic densities (50) ; *(iii)* The vibrations of small structured clusters inside the glass (51) ; *(iv)* The vibrations of localized clusters inside the glass showing elastic fluctuations (52).

Some authors (50,53,54) have connected the Boson peak to the medium distance order inside the glass. The following expression has been proposed (50,55), linking the frequency of the Boson peak ω_{BP} to the correlation size ξ of the structural clusters (thereafter named blobs) :

$$\xi = \frac{V_{av}}{\omega_{BP}}, \tag{1}$$

where V_{av} is the average sound velocity inside the glass and is calculated by the following equation with the longitudinal velocity (V_L) and transversal velocity (V_T).

$$V_{av} = \left(\frac{1}{3V_L^3} + \frac{2}{3V_T^3}\right)^{-1/3} \tag{2}$$

The evolution of the Boson peak intensity is also linked to the heterogeneity of the blobs inside the glass (56,57).

This makes the study of the Boson peak interesting to understand the evolution of the structure at intermediate distance. At the same time, a comparison of the evolution of the Boson peak and the mechanical properties makes this study even more important. Figure 5a represents the evolution of the Boson peak (BP) intensity and Figure 5b the evolution of the BP frequency as a function of the ZnO concentration.

In Figure 5a, a decrease of the intensity with an increase of the ZnO concentration is observed until 5%mol ZnO. Between 5%mol and 15%mol ZnO, an increase of this intensity is noted and finally, a sharp decrease of the intensity is noted for further increase of the ZnO concentration. In Figure 5b, the evolution of the frequency shown as a function of the zinc oxide concentration is stranger. There is a first decrease of the frequency between 0 and 5%mol ZnO and then an increase of the frequency until 15%mol ZnO and a decrease for further concentrations.

The evolution of the intensity of the BP (Figure 5a) could be explained by the change in structural behavior, which will lead to a change in ZnO coordination.

As for the evolution of the Boson peak frequency, in our previous study (24) it was shown that it is more correct to look at the evolution of the blob size than the evolution of the BP frequency alone, which will be done in the discussion part.

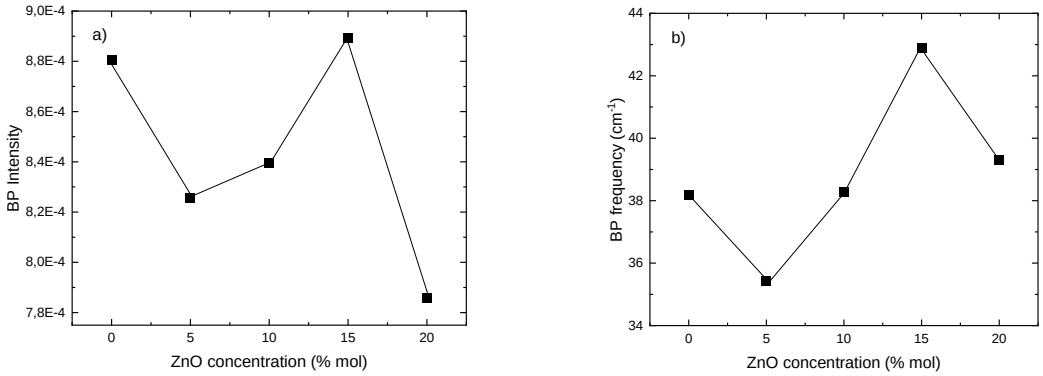

Figure 5: a) BP intensity evolution; b) ω_{BP} evolution as a function of ZnO content.

2.3. Mechanical approach

The mechanical properties were studied by ultrasound echography. The relevant information (Young modulus (E), shear modulus (G), Poisson ratio (ν)) as well as the average sound velocities (Eq.(2)) are calculated from the experimentally obtained longitudinal and transversal velocities (respectively (V_L and V_T)) using

$$E = \rho \frac{3{V_L}^2 - 4{V_T}^2}{\left(\frac{V_L}{V_T}\right)^2 - 1}, \tag{3}$$

$$G = \rho {V_T}^2, \tag{4}$$

$$\nu = \frac{\left(\frac{V_L}{V_T}\right)^2 - 2}{2\left\{\left(\frac{V_L}{V_T}\right)^2 - 1\right\}}, \tag{5}$$

and are reported in Table 3 and Figure 6

Sample	E (GPa)	G (GPa)	Poisson ratio ν	V_L (m.s^{-1})	V_T (m.s^{-1})	V_{av} (m.s^{-1})
TZ0N20	33.6	13.1	0.280	2966	1639	1826
TZ05N15	35.9	14.1	0.274	2998	1673	1863
TZ10N10	39.8	15.8	0.261	3020	1717	1908
TZ15N05	40.2	15.9	0.260	3030	1726	1918
TZ20N0	42.6	16.9	0.256	3055	1750	1944

Table 3 : Young modulus (E), shear modulus (G), Poisson ratio (ν), longitudinal and transversal velocities (respectively (V_L and V_T) values for each sample

The evolution of *E* and *G* (Figure 6a and 6b) shows an overall increase with an increase of the zinc oxide content. There is, though, a slope break after 10%mol ZnO. Looking at the Poisson ratio (Figure 6c), which is inversely proportional to the connectivity of the network (58), an addition of ZnO will overall increase the connectivity of the network. But it is also evident that there is a slope break at 10%mol ZnO, showing once more a different structural behaviour. These results are well in order with the evolution of the structural properties showed previously, showing a change in behaviour at the same concentration in zinc oxide content.

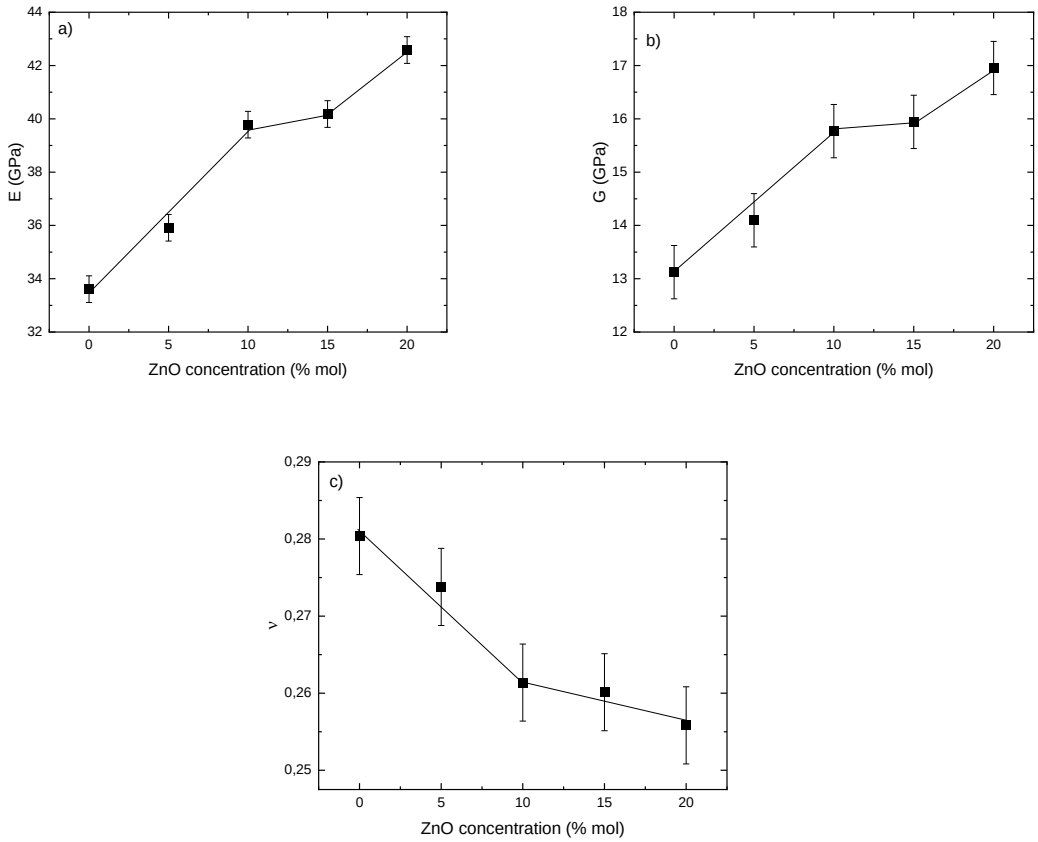

Figure 6 : Evolution of a) the Young modulus (E); b) the shear modulus (G); c) the Poisson ratio (ν) as a function of the ZnO concentration

2.4. Optical properties

Transmission spectra were taken on 2mm thick optically polished pellets. Figure 7 shows the evolution of the transmission of the samples as a function of the wavelength for each sample. TZ0N20 glass showed lower transmission, which is due to macroscopic inhomogeneity of the glass and 2mm thickness. The in-line transmission could be lowered by small refraction of incident light inside the glass.

This evolution is actually easier to understand by knowing the fact that the refractive index of TZ0N20 was measured at different point of the sample and the obtained results showed a larger standard deviation (± 0.04) compared to the other glasses (Fig.8).

The transmission of the other glasses was almost constant, not dependent on the zinc oxide concentration. In the visible to infrared (IR) region, several sharp absorption lines owing to Nd^{3+} ions doped were detected, which were assigned to the optical transitions from $^4I_{9/2}$ level

to 1) $^4I_{13/2}$, 2) $^4I_{15/2}$, 3) $^4F_{3/2}$, 4) $^4F_{5/2}+^2H_{9/2}$, 5) $^4F_{7/2}+^4S_{3/2}$, 6) $^4F_{9/2}$, 7) $^4G_{5/2}+^2G_{7/2}$ and 8) $^2K_{13/2}+^4G_{7/2}+^4G_{9/2}$ levels. (28) A large IR absorption band was attributed to OH vibrations.

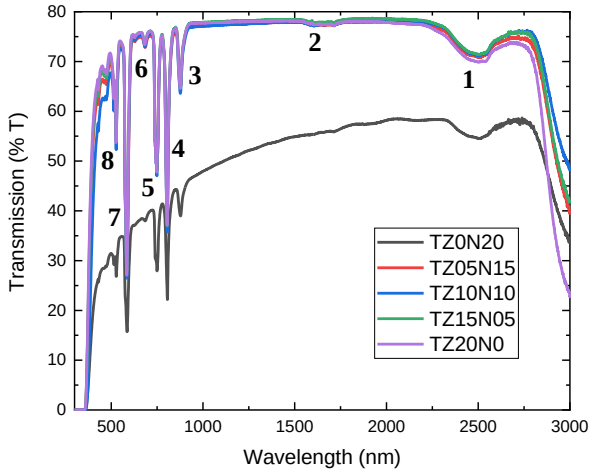

Figure 7 : Transmission spectra of each sample in the wavelength range of 200 to 3000nm. The absorption lines of Nd^{3+} ions in the visible to infrared region were assigned to the optical transitions from $^4I_{9/2}$ level to 1) $^4I_{13/2}$, 2) $^4I_{15/2}$, 3) $^4F_{3/2}$, 4) $^4F_{5/2}+^2H_{9/2}$, 5) $^4F_{7/2}+^4S_{3/2}$, 6) $^4F_{9/2}$, 7) $^4G_{5/2}+^2G_{7/2}$ and 8) $^2K_{13/2}+^4G_{7/2}+^4G_{9/2}$ levels.(28) A large IR absorption band was attributed to OH vibrations.

Refractive indexes of the samples were taken on the same optical flat pellets, with an incident light at 800nm. Table 1 and Figure 8 show the evolution of their values as a function of the sample. The evolution shows that there are two different average values of the refractive index depending on the ZnO concentration. Between 0 and 5%mol ZnO there is a 1.97 average value and for 10%mol ZnO or more there is a 2.02 average value of the refractive index. The latter is preferable to enhancement of third-order nonlinear optical susceptibilities.(4,6) These observations resultantly show that the change in the structural behavior seems to also have an impact on the refractive index value.

Now, looking at the refractive index value of the TZ15N05 glass, it is lower than that of the TZ10N10 and TZ20N0 glass, even if the density of the TZ15N05 glass is the same as the TZ10N10 glass (Table 1), which is not a normal behavior. This evolution could then be interpreted by the increased number of microscopic heterogeneities due to different Zn coordination numbers highlighted in the BP intensity evolution.

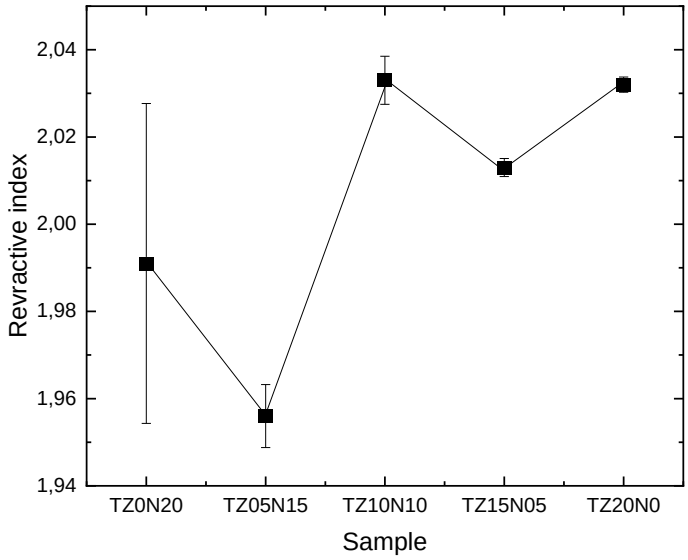

Figure 8 : Evolution of the refractive index as a function of ZnO concentration.

2.5. Discussion

As explained before, *Duval et al*. (55) and *Elliott et al*. (50) independently found a relationship that links the size of density or elastic fluctuations domains ξ (here, called blob size) with the position of the Boson peak frequency ω_{BP} and V_{av}. As a function of the concentration (Fig. 9), an increase in blob size can be noted between 0 and 5%mol ZnO. The blob size then decreases until 15%mol ZnO and increase for further concentrations. An increase in blob size can be associated with an increase of a number of the network linkages due to the different bonding natures of the elements (Te, Zn, and Na) with oxygens and/or the length of the average covalent bonds (Te-O, Zn-O), and vice versa.

It can be seen here that an addition of 5%mol or lower content in ZnO will increase the average number of the networking bonds. This can be explained by the difference between the natures of Na-O and Zn-O bonds. Indeed, Na_2O have ionic bonds in nature, and will not link to the tellurite network. On the contrary, ZnO have covalent bonding characters and will link to the tellurite network, which will increase the average number of the covalent bonds inside the glass.

An increase of 5 to 15%mol ZnO, however, decrease blob size. This can be explained by the fact that ZnO components in six-fold coordination with oxygen, ZnO_6 like ones found in $Zn_2Te_3O_8$ crystal (ZnO_6 (Zn-O: 2.0~2.5 Å) and TeO_4 (Te-O:~1.9 Å with equatorial positioned oxygens and ~2.1 Å with axial bonding oxygens)), are between the tellurite chains and linking them together, which possibly induces a compaction of the glassy system by decreasing contents of the cations by substituting Na_2O with ZnO; the total cation concentration C(x) is varied as 120-x with ZnO concentration x in $80TeO_2$-xZnO-(20-x)Na_2O. A theoretical density linearly increases with ZnO concentration, which was experimentally confirmed as shown in **Table 1**, since the atomic number of Zn (Z=30) is higher than that of Na (Z=11), and thus molar volume should decrease because of the decreasing cation concentration in the glass formula, meaning that the correlation length of the network structures could be shortened with

ZnO concentration. It can be noted in **Table 1** that the estimated molar volume had an overall tendency of the decrease with ZnO concentration. As seen in **Table 3**, the ZnO concentration dependence of the mechanical properties also showed the monotonic increase. However, looking in detail, the molar volume exhibits an anomaly at 10-15%mol (See **Table 1** again) and the mechanical properties appear on the different lines in the border of 10%mol ZnO (**Fig. 6**), as mentioned in the previous session. This is a clue to understand the structural evolution of the TZN glasses.

Further increase in the ZnO content once again increases the size of the blob, which will be associated with an increase in the length of the average bonds of the tellurite glass composed by Te-O and Zn-O as a main framework. By comparing the evolution to the literatures, it might mean that when the ZnO is 4-coordinated and substituting the TeO_2 inside the glass, the difference between the length of the Zn-O and Te-O bond will explain this increase of blob size (Zn-O bond length being longer than Te-O bond length). For example, in $ZnTeO_3$, Zn-O is the bonding length of 1.9~2.3 Å in ZnO_{4+1} unit, while Te-O has ~1.9 Å of trigonal pyramids TeO_3.

By comparing the evolution of the blob size to the structural properties, there should be an increase of blob size between 10 and 15%mol ZnO, which is not the case here. This can be explained by the strong increase of the inhomogeneities between the blobs highlighted with the evolution of the BP intensity and the refractive index values.

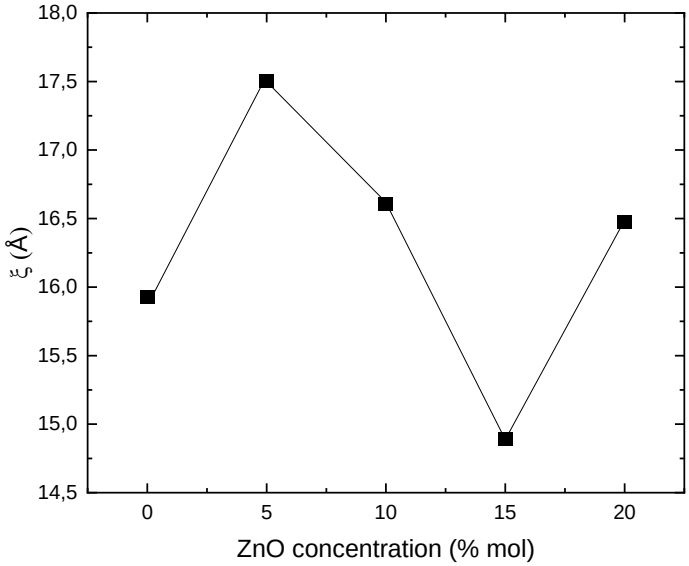

Figure 9 : Evolution of the size of the blobs as a function of the concentration in ZnO

The thermal properties' evolution showed how different the TZ05N15 sample is compared to the other samples, with the lowest intensity of crystallization peak. This goes well with the idea of the fact that really low amount of ZnO content will have a modifier influence. It was also shown that the thermal stability was decreased with further introduction of ZnO content, due to the apparition of a new crystallization peak. This evolution seems to go in favor of a new structural behavior.

The structural evolution as a function of the concentration indicates also a slight influence on the optical properties of the glasses. It has been shown that an addition of more than 10%mol ZnO will change the refractive index value of the glasses.

3. Conclusion

Correlation between structural properties of glasses to different kind of macroscopic physic one has been one of the most important field of research on glasses for years. In this study, some interesting facts have been pointed out.

By comparing mechanical experiments and Raman spectroscopy, it has been possible to understand the structural properties of a glass having a complex structure with two entities that have a coordination number which change as a function of the Na_2O and ZnO content. *(i)* As usual Raman spectroscopy gave information on the change of the Te-O polyedra inside the glass, *(ii)* mechanical experiment gave an understanding on the strength of the different bonds as a function of the concentration, and *(iii)* from both Raman and mechanical experiments by calculating the blobs size, the structural evolution of the glass at intermediate-distance has been evidenced.

This paper showed that for low concentration of ZnO (≤5%mol in this paper), there was not enough zinc oxide content to see the influence of the ZnO as a network former inside the glass, but with an increase of the blob size and TeO_3/TeO_4 ratio, and a decrease of Boson peak intensity. This paper also showed that by increasing the zinc oxide content to 10%mol ZnO, there would be an increase the tellurium polymerization, increase the mechanical properties, decrease of the NBO content and increase the connectivity of the network, resulting in higher refractive index. This indicated that the zinc oxide, which had a 6 coordination, would behave like inside the $Zn_2Te_3O_8$ crystalline phase, linking the tellurite chains together and moreover compacting the glassy system, which were evidenced by the decreasing molar volume. A change in the structural behavior was noted for higher ZnO concentration, associated with an increase of the number of NBO in the tellurium network, an increase of the TeO_3/TeO_4 ratio and a slower increase of the mechanical properties with an increase of ZnO content. This change indicated that the zinc oxide would change its behavior, going toward a 4 coordination, and acting like in the $ZnTeO_3$ crystalline phase by substituting the tellurium inside the chains.

4. Acknowledgement

This work was performed in JSPS KAKENHI Grant Number JP19F19798. The authors of JdeCG and TH gratefully acknowledge the financial support of the Japan Society for the Promotion of Science (JSPS).

Figure Captions

Figure 1 : DTA evolution for every TZN samples. The arrow shows the respective glass transition temperature.

Figure 2 : Raman bands attribution of a typical TZN sample (Example of the TZ15N05 sample)

Figure 3 : Intensity evolution of a) E and F bands and b) G, H, I and J bands as a function of the ZnO concentration

Figure 4 : Evolution of the TeO_3/TeO_4 ratio as a function of the ZnO concentration

Figure 5 : a) BP intensity evolution; b) ω_{BP} evolution as a function of ZnO content.

Figure 6 : Evolution of a) the Young modulus (E); b) the shear modulus (G); c) the Poisson ratio (ν) as a function of the ZnO concentration

Figure 7 : Transmission spectra of each sample in the wavelength range of 200 to 3000nm. The absorption lines of Nd^{3+} ions in the visible to infrared region were assigned to the optical transitions from $^4I_{9/2}$ level to 1) $^4I_{13/2}$, 2) $^4I_{15/2}$, 3) $^4F_{3/2}$, 4) $^4F_{5/2}+^2H_{9/2}$, 5) $^4F_{7/2}+^4S_{3/2}$, 6) $^4F_{9/2}$, 7) $^4G_{5/2}+^2G_{7/2}$ and 8) $^2K_{13/2}+^4G_{7/2}+^4G_{9/2}$ levels.(28) A large IR absorption band was attributed to OH vibrations.

Figure 8 : Evolution of the refractive index as a function of ZnO concentration.

Figure 9 : Evolution of the size of the blobs as a function of the concentration in ZnO

Bibliography

1. El-Mallawany RAH. Tellurite glasses handbook: physical properties and data. 2nd ed. Boca Raton, FL: Taylor & Francis; 2011. 512 p.

2. Mirgorodsky AP, Soulis M, Thomas P, Merle-Méjean T, Smirnov M. *Ab initio* study of the nonlinear optical susceptibility of TeO_2-based glasses. Phys Rev B [Internet]. 2006 Apr 28;73(13).

3. Wang JS, Vogel EM, Snitzer E. Tellurite glass: a new candidate for fiber devices. Opt Mater. 1994 Aug;3(3):187–203.

4. Kim S-H, Yoko T, Sakka S. Linear and Nonlinear Optical Properties of TeO_2 Glass. J Am Ceram Soc. 1993 Oct;76(10):2486–90.

5. Soulis M, Merle-Méjean T, Mirgorodsky AP, Masson O, Orhan E, Thomas P, et al. Local molecular orbitals and hyper-susceptibility of TeO_2 glass. J Non-Cryst Solids. 2008 Jan;354(2–9):199–202.

6. Duclère J-R, Hayakawa T, Roginskii EM, Smirnov MB, Mirgorodsky A, Couderc V, et al. Third order nonlinear optical properties of a paratellurite single crystal. J Appl Phys. 2018 May 14;123(18):183105.

7. Sarjeant PT, Roy R. New Glassy and Polymorphic Oxide Phases Using Rapid Quenching Techniques. J Am Ceram Soc. 1967 Oct;50(10):500–3.

8. Udovic M, Thomas P, Mirgorodsky A, Durand O, Soulis M, Masson O, et al. Thermal characteristics, Raman spectra and structural properties of new tellurite glasses within the Bi_2O_3–TiO_2–TeO_2 system. J Solid State Chem. 2006 Oct;179(10):3252–9.

9. Udovic M, Thomas P, Mirgorodsky A, Masson O, Merle-Mejean T, Lasbrugnas C, et al. Formation domain and characterization of new glasses within the Tl_2O–TiO_2–TeO_2 system. Mater Res Bull. 2009 Feb;44(2):248–53.

10. Linda D, Dutreilh-Colas M, Hamani D, Thomas P, Mirgorodsky A, Duclère J-R, et al. New glasses within the Tl_2O–Ag_2O–TeO_2 system: Thermal characteristics, Raman spectra and structural properties. Mater Res Bull. 2010 Dec;45(12):1816–24.

11. Noguera O, Merle-Méjean T, Mirgorodsky AP, Thomas P, Champarnaud-Mesjard J-C. Dynamics and crystal chemistry of tellurites. II. Composition- and temperature-dependence of the Raman spectra of $x(Tl_2O)+(1-x)Te_2O$ glasses: evidence for a phase separation? J Phys Chem Solids. 2004 May;65(5):981–93.

12. Dutreilh-Colas M, Charton P, Thomas P, Armand P, Marchet P, Champarnaud-Mesjard JC. The TeO_2 -rich part of the TeO_2–Ga_2O_3 system: equilibrium and non-equilibrium phase diagram. J Mater Chem. 2002;12(9):2803–6.

13. Blanchandin S, Thomas P, Marchet P, Champarnaud-Mesjard JC, Frit B. New heavy metal oxide glasses: investigations within the TeO_2–Nb_2O_5–Bi2O3 system. J Alloys Compd. 2002 Dec;347(1–2):206–12.

14. Jeansannetas B, Blanchandin S, Thomas P, Marchet P, Champarnaud-Mesjard JC, Merle-Méjean T, Frit B, Nazabal V, Fargin E, Le Flem G, Martin M.O, Bousquet B, Canioni L, Le Boiteux S, Segonds P, Sarger L. Glass Structure and Optical Nonlinearities in Thallium(I) Tellurium(IV) Oxide Glasses. J Solid State Chem. 1999 Sep;146(2):329–35.

15. Soulis M, Mirgorodsky AP, Merle-Méjean T, Masson O, Thomas P, Udovic M. The role of modifier's cation valence in structural properties of TeO_2-based glasses. J Non-Cryst Solids. 2008 Jan;354(2–9):143–9.

16. Zaki MR, Hamani D, Dutreilh-Colas M, Duclère J-R, Masson O, Thomas P. Synthesis, thermal, structural and linear optical properties of new glasses within the TeO_2-TiO_2-WO_3 system. J Non-Cryst Solids. 2018 Mar;484:139–48.

17. Ahmmad S kareem, Samee MA, Edukondalu A, Rahman S. Physical and optical properties of zinc arsenic tellurite glasses. Results Phys. 2012;2:175–81.

18. Van Uitert LG, Wemple SH. $ZnCl_2$ glass: A potential ultralow–loss optical fiber material. Appl Phys Lett. 1978 Jul;33(1):57–9.

19. Sekiya T, Mochida N, Ohtsuka A. Raman spectra of MO–TeO_2 (M = Mg, Sr, Ba and Zn) glasses. J Non-Cryst Solids. 1994 Feb;168(1–2):106–14.

20. Bürger H, Kneipp K, Hobert H, Vogel W, Kozhukharov V, Neov S. Glass formation, properties and structure of glasses in the TeO_2–ZnO system. J Non-Cryst Solids. 1992 Dec;151(1–2):134–42.

21. Duverger C, Bouazaoui M, Turrell S. Raman spectroscopic investigations of the effect of the doping metal on the structure of binary tellurium-oxide glasses. J Non-Cryst Solids. 1997 Nov;220(2–3):169–77.

22. Hoppe U, Yousef E, Rüssel C, Neuefeind J, Hannon AC. Structure of zinc and niobium tellurite glasses by neutron and x-ray diffraction. J Phys Condens Matter. 2004;16(9):1645.

23. Kozhukharov V, Bürger H, Neov S, Sidzhimov B. Atomic arrangement of a zinc-tellurite glass. Polyhedron. 1986 Jan 1;5(3):771–7.

24. de Clermont-Gallerande J, Dutreilh-Colas M, Célarié F, Gueguen Y, Bergler M, de Ligny D, et al. Correlation between mechanical and structural properties as a function of temperature within the TeO_2–TiO_2–ZnO ternary system. J Non-Cryst Solids. 2020 Jan;528:119716.

25. Thorbahn JG, Zwanziger JW. Compositional dependence of the stress-optic response in zinc tellurite glasses. J Non-Cryst Solids. 2013 Dec;381:48–53.

26. Ghribi N, Dutreilh-Colas M, Duclère J-R, Hayakawa T, Carreaud J, Karray R, et al. Thermal, optical and structural properties of glasses within the TeO_2TiO_2ZnO system. J Alloys Compd. 2015 Feb;622:333–40.

27. ASTM International. Standard Test Method for Dynamic Young's Modulus, Shear Modulus and Poisson's Ratio by Impulse Excitation of Vibration. ASTM E1876- 01; 2006.

28. de Clermont-Gallerande J, Saito S, Hayakawa T, Colas M, Duclère J-R, Thomas P. Optical properties of Nd^{3+}-doped TeO_2-TiO_2-ZnO glasses with lower hydroxyl content. J Non-Cryst Solids. 2020 Jan;528:119678.

29. D. de Sousa Menses. FOCUS version 1.0, software utility for the creation of optical function.

30. Ghribi N, Dutreilh-Colas M, Duclère J-R, Gouraud F, Chotard T, Karray R, et al. Structural, mechanical and optical investigations in the TeO_2-rich part of the TeO_2–GeO_2–ZnO ternary glass system. Solid State Sci. 2015 Feb;40:20–30.

31. Phillips WA. Amorphous Solids: Low-Temperature Properties [Internet]. Berlin, Heidelberg: Springer Berlin Heidelberg; 1981 [cited 2019 May 14]. Available from: http://public.eblib.com/choice/publicfullrecord.aspx?p=3095186

32. Nakayama T. Boson peak and terahertz frequency dynamics of vitreous silica. Rep Prog Phys. 2002 Aug 1;65(8):1195–242.

33. Pohl RO, Liu X, Thompson E. Low-temperature thermal conductivity and acoustic attenuation in amorphous solids. Rev Mod Phys. 2002 Oct 30;74(4):991–1013.

34. Schirmacher W, Diezemann G, Ganter C. Harmonic Vibrational Excitations in Disordered Solids and the "Boson Peak." Phys Rev Lett. 1998 Jul 6;81(1):136–9.

35. Taraskin SN, Loh YL, Natarajan G, Elliott SR. Origin of the Boson Peak in Systems with Lattice Disorder. Phys Rev Lett. 2001 Feb 12;86(7):1255–8.

36. Grigera TS, Martín-Mayor V, Parisi G, Verrocchio P. Phonon interpretation of the 'boson peak' in supercooled liquids. Nature. 2003 Mar;422(6929):289–92.

37. Parisi G. On the origin of the boson peak. J Phys Condens Matter. 2003 Mar 26;15(11):S765–74.

38. Lubchenko V, Wolynes PG. The origin of the boson peak and thermal conductivity plateau in low-temperature glasses. Proc Natl Acad Sci. 2003 Feb 18;100(4):1515–8.

39. Gurevich VL, Parshin DA, Schober HR. Anharmonicity, vibrational instability, and the Boson peak in glasses. Phys Rev B. 2003 Mar 17;67(9):094203.

40. Gurevich VL, Parshin DA, Schober HR. Pressure dependence of the boson peak in glasses. Phys Rev B [Internet]. 2005 Jan 28 [cited 2018 Jan 31];71(1). Available from: https://link.aps.org/doi/10.1103/PhysRevB.71.014209

41. Pilla O, Caponi S, Fontana A, Gonçalves JR, Montagna M, Rossi F, et al. The low energy excess of vibrational states in v-SiO_2 : the role of transverse dynamics. J Phys Condens Matter. 2004 Dec 1;16(47):8519–30.

42. Gurarie V, Altland A. Phonons in Random Elastic Media and the Boson Peak. Phys Rev Lett. 2005 Jun 22;94(24):245502.

43. Johari GP. Librational heat capacity of fullerenes in the Einstein model. J Chem Phys. 2003 Dec 8;119(22):11912–6.

44. Johari GP. Molecular inertial effects in liquids: Poley absorption, collision-induced absorption, low-frequency Raman spectrum and Boson peaks. J Non-Cryst Solids. 2002 Sep;307–310:114–27.

45. Power G, Johari GP, Vij JK. Relaxation strength of localized motions in D-sorbitol and mimicry of glass-softening thermodynamics. J Chem Phys. 2003 Jul;119(1):435–42.

46. Chumakov AI, Sergueev I, van Bürck U, Schirmacher W, Asthalter T, Rüffer R, et al. Collective Nature of the Boson Peak and Universal Transboson Dynamics of Glasses. Phys Rev Lett. 2004 Jun 18;92(24):245508.

47. Yannopoulos SN, Papatheodorou GN, Fytas G. Low-energy excitations in noncrystalline arsenic trioxide. J Chem Phys. 1997 Aug;107(5):1341–9.

48. Greaves GN. Identifying Vibrations That Destabilize Crystals and Characterize the Glassy State. Science. 2005 May 27;308(5726):1299–302.

49. Martin AJ, Brenig W. Model for Brillouin Scattering in Amorphous Solids. Phys Status Solidi B. 1974 Jul 1;64(1):163–72.

50. Elliott SR. A Unified Model for the Low-Energy Vibrational Behaviour of Amorphous Solids. Europhys Lett EPL. 1992 Jun 1;19(3):201–6.

51. Phillips JC. Topology of covalent non-crystalline solids II: Medium-range order in chalcogenide alloys and A□Si(Ge). J Non-Cryst Solids. 1981 Jan;43(1):37–77.

52. Pang T. Local vibrational states of glasses. Phys Rev B. 1992 Feb 1;45(5):2490–2.

53. Malinovsky VK, Sokolov AP. The nature of boson peak in Raman scattering in glasses. Solid State Commun. 1986 Mar;57(9):757–61.

54. Takahashi Y, Osada M, Masai H, Fujiwara T. Anomalous Boson Behavior and Nanometric Heterogeneity in Glassy Fresnoite. Appl Phys Express. 2008 Dec 12;1:121901.

55. Duval E, Boukenter A, Achibat T. Vibrational dynamics and the structure of glasses. J Phys Condens Matter. 1990 Dec 31;2(51):10227–34.

56. Duval E, Saviot L, Mermet A, David L, Etienne S, Bershtein V, et al. Inelastic light, neutron, and X-ray scattering related to the heterogeneous elasticity of glasses. J Non-Cryst Solids. 2002 Sep;307–310:103–8.

57. Champagnon B, Wondraczek L, Deschamps T. Boson peak, structural inhomogeneity, light scattering and transparency of silicate glasses. J Non-Cryst Solids. 2009 May;355(10–12):712–4.

58. Greaves GN, Greer AL, Lakes RS, Rouxel T. Poisson's ratio and modern materials. Nat Mater. 2011 Nov;10(11):823–37.